AAPS PharmSciTech (© 2018)
DOI: 10.1208/s12249-017-0946-3

Research Article

Structural Elucidation of Poloxamer 237 and Poloxamer 237/Praziquantel Solid Dispersions: Impact of Poly(Vinylpyrrolidone) over Drug Recrystallization and Dissolution

Silvina Orlandi,[1] Josefina Priotti,[1] Hermínio P. Diogo,[2] Dario Leonardi,[1] Claudio J. Salomon,[1,3] and Teresa G. Nunes[2,3]

Received 7 November 2017; accepted 21 December 2017

Abstract. Praziquantel (PZQ) is the recommended, effective, and safe treatment against all forms of schistosomiasis. Solid dispersions (SDs) in water-soluble polymers have been reported to increase solubility and bioavailability of poorly water-soluble drugs like PZQ, generally due to the amorphous form stabilization. In this work, poloxamer (PLX) 237 and poly(vinylpyrrolidone) (PVP) K30 were evaluated as potential carriers to revert PZQ crystallization. Binary and ternary SDs were prepared by the solvent evaporation method. PZQ solubility increased similarly with PLX either as binary physical mixtures or SDs. Such unpredicted data correlated well with crystalline PZQ and PLX as detected by solid-state NMR (ssNMR) and differential scanning calorimetry in those samples. Ternary PVP/PLX/PZQ SDs showed both ssNMR broad and narrow superimposed signals, thus revealing the presence of amorphous and crystalline PZQ, respectively, and exhibited the highest PZQ dissolution efficiency (up to 82% at 180 min). SDs with PVP provided a promising way to enhance solubility and dissolution rate of PZQ since PLX alone did not prevent recrystallization of amorphous PZQ. Based on ssNMR data, novel evidences on PLX structure and molecular dynamics were also obtained. As shown for the first time using ssNMR, propylene glycol and ethylene glycol constitute the PLX amorphous and crystalline components, respectively.

KEY WORDS: praziquantel; poloxamer; PVP; solid dispersions; DSC; solid-state NMR.

INTRODUCTION

Schistosomiasis, or bilharzia, is a parasitic disease caused by trematode flatworms of the genus *Schistosoma*. According to the World Health Organization (1), people get infected when exposed to contaminated water and schistosomiasis transmission has been reported from 78 countries. In 2014, nearly 258 million people needed treatment to reduce and prevent morbidity. Praziquantel (PZQ; Scheme 1), 2-(cyclohexylcarbonyl)-1,2,3,6,7,11b–hexahydro-4H-pyrazino[2,1-a]isoquinolin-4-one, is the recommended effective and safe treatment against all forms of schistosomiasis (2). Nevertheless, some physical properties of this low-cost drug require adopting novel strategies.

PZQ is classified in class II in the Biopharmaceutics Classification Systems because it has very low water solubility which gives rise to a low bioavailability when administered orally (3). Due to its low solubility in water and its extensive first-pass hepatic (4,5), large doses are required because PZQ is administered as a racemic compound and only the *R* enantiomer has therapeutic efficacy. *S*-PZQ is merely responsible for the bad taste of the drug (6). Thus, several approaches have been proposed to improve PZQ aqueous solubility, dissolution rate, and bioavailability. Mechanochemical activation in vibrational mill with poly(vinylpyrrolidone) (PVP, Scheme 1), among other pharmaceutical excipients, was recently employed to boost water solubility of PZQ; all coground systems presented a high amorphous degree and solubility remarkably higher than the raw drug (7). Another promising route to achieve such goals involves preparing inclusion complexes of PZQ and β-cyclodextrin derivatives (8). Solid dispersions (SDs) were previously reported as successful approaches (4). For example, SDs prepared with hydrogenated castor oil improved PZQ dissolution rate and intestinal absorption (9). SDs based on polymeric materials

Electronic supplementary material The online version of this article (https://doi.org/10.1208/s12249-017-0946-3) contains supplementary material, which is available to authorized users.

[1] IQUIR-CONICET, Facultad de Ciencias Bioquímicas y Farmacéuticas, Área Técnica Farmacéutica, Universidad Nacional de Rosario, Suipacha 531, Rosario, Argentina.
[2] CQE, Instituto Superior Técnico, Universidade de Lisboa, Av. Rovisco Pais, 1049-001, Lisbon, Portugal.
[3] To whom correspondence should be addressed. (e–mail: csalomon@fbioyf.unr.edu.ar; teresa.nunes@ist.utl.pt)

Published online: 08 January 2018

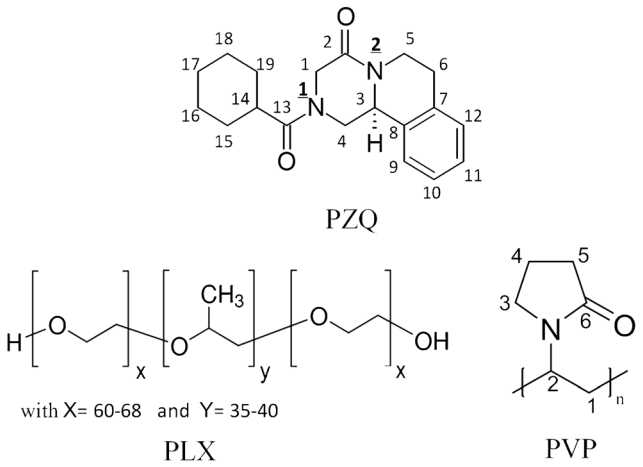

Scheme 1. Molecular structures of PZQ, PLX, and PVP, with the carbon numbering followed in the present study

have been considered the most important advance. They can be prepared either by solvent evaporation (10) or by using the fusion method (11). SDs are expected to increase drug dissolution mainly due to the amorphous form stabilization (12). However, the recrystallization process may occur.

To date, SD is one of the most widely investigated approaches for the improvement of drug dissolution profile of poorly aqueous-soluble drugs (13–15). Usually, SDs are prepared through the dissolution of the hydrophilic polymer, as carrier matrix, and the hydrophobic drug using a single solvent or a corresponding mixture of solvents including water, ethanol, and acetone (16). Even though such solvents are the most widely used to formulate SDs, unpredicted solvent effect was reported for the first time on the preparation of PZQ/PVP SDs: the formation of PZQ amorphous and crystalline phases induced by ethanol and water, respectively (17). Using differential scanning calorimetry (DSC) and solid-state NMR (ssNMR), among other techniques, a significant crystalline PZQ content was detected at high PVP concentration, with no correlation with the drug saturation solubility data (17). In the last decades, another type of polymeric structures has been applied to optimize the performance of SDs. Poloxamers (PLXs) are nonionic triblock semi-crystalline copolymers containing two hydrophilic chains (polyethylene glycol, PEG) connected to one hydrophobic chain (polypropylene glycol, PPG) (18). PLXs have surfactant properties due to their amphiphilic structure, making them appropriate to improve the solubility of several drugs (19), along with other applications. For example, shielding the surface of polymer nanoparticles with PLX makes them compatible with the physiological function of lung surfactant, thus providing a novel approach for colloidal drug delivery (20). In aqueous environments, individual block copolymers (unimers) are present while aggregation of unimers occurs, forming micelles, above the critical micelle temperature and concentration (18). This process is driven by the dehydration of the hydrophobic PPG, which becomes less soluble with concentration and temperature increases. Micelles contain PPG (insoluble) in the core and PEG (soluble) in the shells enabling to minimize PPG solvent interactions (18). Very low toxicity and higher drug solubilizing capacity are reported on PLXs with high PEG content (18). PVP K30/PLX-188 were used as carriers for the preparation of SDs of poor water-soluble drugs by solvent evaporation (21), spray-drying (22), or hot melt extrusion (23), and the API solubility was enhanced because of the inclusion of PLX-188 into the PVP matrix. In particular, it has been reported that the drug, partially amorphous, is dispersed in PVP while poloxamer acts as a plasticizer by lowering the glass transition temperature (T_g) of PVP (23). The drug physical stability and dissolution performance are expected to be controlled by the morphology and microstructure of crystalline drug/polymer SDs. It was noticed that PEG, PPG, and PLX could all significantly improve the crystallization rate of drugs, because of the largely reduced T_g of SDs by those low T_g polymers (24). Accordingly, the crystallization mechanism of acetaminophen within PLX and homopolymers PEG and PPG has been investigated and the microstructure of various SDs of acetaminophen and bifonazole in those polymers was characterized by DSC and other techniques (24).

The key goal of this study was to get structural insights into ternary SDs containing PZQ and a combination of PVP K30 with PLX (PLX 237) as carrier. To pursue this investigation, PLX and binary PLX/PZQ SDs were studied, also. Another main purpose was to evaluate binary and ternary SDs as PZQ dissolution enhancers, aiming to correlate these data with the presence of amorphous PZQ. PLXs are available with various molecular weights and relative proportions of EG *versus* PG units. PLX 237 contains PEG with 60–68 EG units connected to PPG with 35–40 PG units (18) (Scheme 1). PLX 237 has an average molecular weight of 6.84–8.83 kDa, around 70% by weight of EG (the last of the three digits times 10), and an average molecular weight of PPG of about 2.3 kDa (the first two digits multiplied by 100) (18).

It is worth mentioning that, to the best of our knowledge, the formulation of PLX-237/PZQ and PVP K30/PLX-237/PZQ SDs binary and ternary SDs, respectively, has not been investigated.

MATERIALS AND METHODS

Materials

Racemic Praziquantel (PZQ, $C_{19}H_{24}N_2O_2$, purity > 99.4%) was purchased from Romikin (Buenos Aires, Argentina). Poly(vinylpyrrolidone) powder (PVP K30, average MW 40,000) and poloxamer 237 (PLX 237, average MW 6840–8830) were purchased from BASF SE (Ludwigshafen, Germany). All the reagents and chemicals used for analytical purpose were of chromatography grade.

Methods

Preparation of Solid Dispersions and Physical Mixtures

(A) Solid binary dispersion (SD) of PLX/PZQ at 1:1 (*w*/*w*) was prepared by the solvent evaporation method. PZQ (150 mg) was dissolved in 10 ml of ethanol while the polymer (150 mg) was dissolved in 10 ml of water. The solutions were mixed under magnetic stirring for 30 min at room temperature. The solvents were then evaporated under reduced pressure, dried at 40°C (48 h), passed through

100 mesh sieve and stored in a desiccator. (B) Ternary SDs of PVP/PLX/PZQ at 1:1:1 and 2:1:1 (*w*/*w*/*w*) were also prepared dissolving both polymeric components in water and PZQ in ethanol using the procedure already described.

Physical mixtures (PMs) of PLX/PZQ and PVP/PLX/PZQ, at 1:1 and 1:1:1 or 2:1:1 weight ratios, were prepared by physically mixing the components thoroughly for 10 min in a mortar until a homogeneous mixture has been obtained. The powder was then passed through 100 mesh sieve and stored in a desiccator.

Dissolution Studies

The dissolution studies of pure PZQ, SDs, and PMs were performed using a Standard Dissolution Apparatus II Hanson Research SR8 Plus (Chatsworth, USA). Samples containing 150 mg of PZQ were added to 900 ml of medium (0.1 N HCl, 2 mg/ml sodium lauryl sulfate) and thermostated at 37 ± 0.1°C with paddle rotating at 50 rpm (25). Aliquots were taken at 10, 20, 30, 60, 90, 120 and 180 min and filtered through a membrane filter (0.45 μm). It was replaced by the same volume of dissolution medium to maintain a constant volume. Concentration of PZQ was determined spectrophotometrically at $\lambda = 263$ nm. All the experiments were carried out in triplicate.

Dissolution efficiency (DE) was calculated from the area under the dissolution curve up to a certain time t and expressed as percentage of the area of the rectangle defined by y_{100} (ordinate) and t (abcissa) according to the following equation:

$$\%\mathrm{DE} = \frac{\int_0^t y \times dt}{y_{100} \times t} \times 100 \tag{1}$$

where y is the percentage of PZQ dissolved at the time interval dt and y_{100} corresponds to the maximum PZQ dissolved in the same time t, that is to 100% dissolution. The area under dissolution curve was performed using GraphPad Prism version 5.00 for Windows, GraphPad Software (San Diego, CA). It was observed that PVP and PLX did not interfere with this assay at 263 nm. A one-way ANOVA followed by the Tukey's test for multiple comparisons was performed. Differences with a P value < 0.05 were considered significant.

Differential Scanning Calorimetry

The thermal behavior of pure components, SDs and PMs, was achieved with a 2920MDSC system from TA Instruments Inc. operated as a conventional DSC. The temperature and heat flow scales of the apparatus were performed as described (26), using high-purity standards. Three samples of each pure component, SD and PM, were used to evaluate the reproducibility of the corresponding thermal profile. Samples with mass in the range 3 to 8 mg were placed into aluminum pans nonhermetically sealed and weighed in a Mettler UMT2 ultra-micro balance. The measuring cell was continually purged with high purity helium gas (Air Liquide N55) at a flow rate of 30 cm^3 min^{-1}. An empty aluminum pan, identical to those used for the samples, was used as reference. Cooling has been achieved with the liquid nitrogen cooling accessory (LNCA from TA) which provides automatic and continuous programmed sample cooling down. The experimental protocol was as follows: (a) PLX sample (Scheme 1) was firstly equilibrated at $T = -110$°C and then heated up to 80°C and cooling again, and (b) all the other samples were firstly equilibrated at −100°C and then heated till 210°C. The heat flow curves were obtained in the first ramp and in all DSC runs a heating rate of 10°C/min was selected. All the data were analyzed using Universal Analysis Software from TA.

Solid-State NMR Spectroscopy

The solid-state spectra were acquired using a Tecmag Redstone/Bruker 300WB spectrometer. Powdered samples (about 200 mg) were packed into 7 mm o.d. zirconia rotors, equipped with Kel-F caps. A spherical Kel-F insert suitable for these rotors was used when an appropriate sample amount was not available (in general ~ 100 mg). ^{1}H magic angle spinning (MAS) spectra were recorded at 300.16 MHz using one 90° RF pulse (Bloch decay) of 5 μs and 5 s relaxation delay. The spinning rate was 3.2 kHz. ^{13}C cross-polarization/MAS (CP/MAS) spectra were obtained at 75.49 MHz with a spinning rate of 3.1 kHz, unless indicated otherwise. Contact time of 3 ms, 90° RF pulses of about 4 μs, and 5 s relaxation delays were selected. When necessary, ^{13}C spinning sidebands were suppressed using the TOSS sequence (TOtal Suppression of Spinning Sidebands) (27).

The proton relaxation time in the rotating frame ($^{H}T_{1\rho}$) and the time constant for the CP build-up (TCH) were measured using ^{13}C CP/MAS experiments by recording the intensity of the carbon signals as a function of the variable CP duration. A frequency field of 62.5 kHz was used for the spin-lock field B_1. The recycling delay was 5 s, and the number of transients was 84. The contact time ^{1}H-^{13}C (t_c) was consecutively increased from 300 μs to 100 ms (28 values) in a series of experiments and the magnetization recorded from each carbon species was plotted against t_c. The data were analyzed by a nonlinear least-squares fit of the right-hand side of Eq. 2.

$$y = I_0\left[1-\left(T_{\mathrm{CH}}/{}^{\mathrm{H}}T_{1\rho}\right)\right]^{-1}\left[\exp\left(-t/{}^{\mathrm{H}}T_{1\rho}\right)-\exp(-t/T_{\mathrm{CH}})\right] \tag{2}$$

where I_0 is the absolute amplitude, which is proportional to the magnetization at thermal equilibrium (28). In addition, $^{H}T_{1\rho}$ data were measured by recording the ^{13}C signal as a function of the ^{1}H spin-locking time t, before the CP period; t was selected between 10 μs and 14 ms (17 values). The frequency field of the spin-locking field B_1 was kept at 62.5 kHz. Spectra were run with 5 s recycle delay and, to minimize spin-diffusion during measurements, t_c was only 400 μs. $^{H}T_{1\rho}$ data were obtained using Eq. 3:

$$y = I_0\left[\exp\left(-t/{}^{\mathrm{H}}T_{1\rho}\right)\right] \tag{3}$$

Equation 3 was fitted to the experimental data (signal intensity as a function of t), using the least-squares method. Relaxation data were always measured at about 20°C.

^{1}H and ^{13}C chemical shifts were referenced with respect to external tetrakis(trimethylsilyl)silane and glycine, respectively (^{1}H and ^{13}CO observed at 0.097 and 176.03 ppm, respectively).

Gaussian functions were selected to iteratively deconvolute relevant signals in ^{13}C MAS and CP/MAS spectra by the least-squares method using the software Origin (Microcal Software, Inc., USA).

RESULTS AND DISCUSSION

Dissolution Studies

Dissolution performances of PZQ were evaluated as binary and ternary PZQ samples and as pure drug. Figure 1 shows the dissolution rate of raw PZQ, PZQ in solid dispersions (SDs), and PZQ in physical mixtures (PMs).

As observed in Fig. 1, dissolution of raw PZQ has increased from 33.2 to 57.0% after 30 and 180 min, respectively. In the case of PLX/PZQ samples, both PMs and SDs showed similar enhanced PZQ dissolution efficiency and dissolution rate as compared with raw PZQ. The impact of PLX over the dissolution of PZQ as SD would be related with a potential micellar solubilization and/or the reduction of the hydrophobic interaction between such components. PMs are expected to increase drug dissolution due to maximizing the PZQ surface area in contact with the solvent. It must be pointed out here that no significant differences were noticed when comparing ssNMR spectra of PLX/PZQ as PM and SD (see Fig. S5, *Supplementary Material*). On the other hand, ternary PZQ SD samples exhibited higher DE compared to binary systems (up to 82% within 180 min). Significant differences were found between PLX/PZQ 1:1 (DS) and PVP/PLX/PZQ 1:1:1 (DS) ($P = 0.02$) and also between PLX/PZQ 1:1 (DS) and PVP/PLX/PZQ 2:1:1 (DS) ($P = 0.01$). The hydrophilic character of PVP could increase drug wettability and reduce interfacial tension between PZQ and dissolution media (29,30). DSC and solid-state NMR were subsequently used, aiming to elucidate those unpredicted data. Firstly, the drug and the carriers were characterized.

DSC and Solid-State NMR Studies of the Carriers and PZQ

DSC of PLX, PVP, and PZQ

The glass transition (T_g) and the melting temperatures (T_m) of PLX were detected at −61 and 49°C, respectively (Fig. S1, *Supplementary Material*); T_g and T_m are the thermal signatures expected for a semi-crystalline copolymer. The T_g of PVP K30 was detected at 156°C (17) or 165.03°C (31). Chemical purity of the racemic crystalline PZQ has been previously confirmed by DSC (the values obtained for T_{onset}, T_{max}, and enthalpy of fusion were, respectively, 138.16°C, 142.52°C, and 94.19 J/g) along with liquid chromatography-mass spectrometry (98.9%); the T_g was detected at 40°C (17).

Solid-State NMR of PLX, PVP, and PZQ

Structural and Molecular Mobility Studies of PLX. Solid-state NMR is expected to reveal the structural complexity that characterizes a semi-crystalline copolymer like PLX. Therefore, pure PLX has been studied prior to PLX/PZQ and PLX/PVP/PZQ formulations. ^{1}H and ^{13}C spectra were acquired from PLX either in static or under MAS modes.

Figure 2 shows the ^{1}H MAS spectrum of PLX. The resonances (δ 1.07, 3.31, and 3.47 ppm) are assigned to CH_3, CH_2, and CH from PPG units, respectively; the signal at 3.31 ppm (shoulder) includes the contribution from PEG methylene groups. Other much less intense peaks are from spinning side bands. Such weaker signals are consistent with the presence of a polymer in the rubber temperature region because the ^{1}H spectrum was recorded at 20°C, that is about 80°C above T_g (−61°C; Fig. S1, *Supplementary Material*). It is worth mentioning here that the intensity of PEG signal does not correlate with the number of EG units in PLX chain (about 60–68 units against 35–40 PG units, as shown in Scheme 1). Clearly, part of ^{1}H magnetization from CH_2 in EG units was not recorded, possibly because EG is mainly present in ordered domains and the corresponding homonuclear (H–H) dipolar interaction is very high due to the short interproton distance (0.17 nm); the corresponding dipolar coupling constant and dipolar splitting are 25 and 50 kHz, respectively. In the present study, signals had remained too broad to be detected because the homonuclear dipolar interaction was not removed at the selected spinning rate. Hence, further NMR experiments were performed to clarify this issue.

^{13}C CP NMR spectra obtained from PLX either in the static or under MAS modes are shown in Fig. 2 (right side). The resonances of PPG carbon nuclei have been recorded at 75.29 ppm (CH), 73.43 ppm (CH_2), and 17.67 ppm (CH_3). The broad peak at about 71.7 ppm is assigned to the PEG methylene group.

The spectrum recorded under static mode (Fig. 2) has been deconvoluted using three Gaussian functions with the following parameters: (1) δ 17.57 ± 0.01 ppm, full width at half maximum (FWHM) 2.35 ± 0.02 ppm, integral 2.04 ± 0.01 arbitrary units (a.u.), (2) δ 74.29 ± 0.01 ppm, FWHM 4.08 ± 0.03 ppm, integral 4.11 ± 0.04 a.u.; and (3) δ 70.68 ± 0.10 ppm, FWHM 13.78 ± 0.16 ppm, integral 4.03 ± 0.06 a.u.. The high mobility of the methyl group is reflected in the line shape of its signal (symmetric peak with low FWHM). The highest chemical shift anisotropy, probed by FWHM, is expected from carbon nuclei in rigid, ordered lamellae. Oriented PEG units (at δ 70.68 ± 0.10 ppm) present the highest FWHM. Therefore, PEG is considered the dominant contribution to the PLX crystalline regions.

^{13}C CP/MAS spectra of PLX run with different CP contact times (t_c) are shown in Fig. 2, and the influence of t_c is clearly exposed. The PEG signal is the major contribution at low t_c (300 μs). However, once t_c has been increased to 1 ms, the most intense peaks became those from PPG. The influence of t_c in the peak intensity reveals that the PPG chain has higher mobility than the PEG chain. Therefore, it is hypothesized here that PPG constitutes the amorphous component of PLX and the PLX crystallinity may be associated to short range order of some PEG units. Relaxation studies, which are described next, support this assumption.

The influence of t_c has been previously reported on ^{13}C CP/MAS spectra obtained from nanosuspensions of PLX 407 and piroxicam, which have been prepared by the wet milling

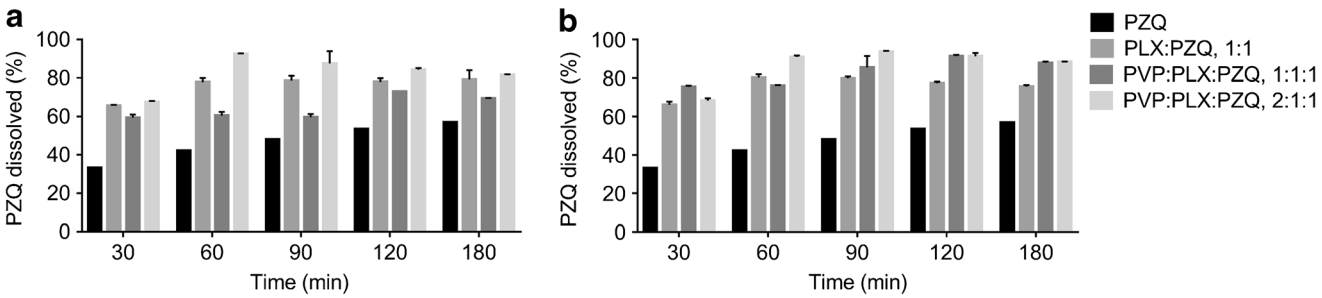

Fig. 1. Histograms of dissolution rates. **a** PMs. **b** SDs

method (32). Unlike in the solid-state data presented here, the results were consistent with higher mobility of PEO chain in the nanoparticles compared with PPO, as expected on the basis of the PEO hydrophilic character (32).

Molecular mobility in amorphous and crystalline PLX regions is expected to be related to different frequency ranges, which NMR relaxation studies enable probing. Spin-lattice relaxation time in the rotating frame ($T_{1\rho}$) depends on motions on the kHz frequency scales. $^{H}T_{1\rho}$ depends also on spin H–H diffusion, an energy conservative process that may mask mobility data. This process is particularly relevant for hydrogen nuclei, due to both high isotopic natural abundance and gyromagnetic ratio, and when long relaxation times are under measurement (like spin-lattice relaxation time, T_1).

Relaxation studies have been performed at about 20°C, that is at least at 80°C higher than T_g (−61°C; Fig. S1, *Supplementary Material*). Two different experiments have been performed. Firstly, the time constants for the ^{13}C magnetization build-up under CP (*T*CH) have been obtained, as well as $T_{1\rho}$ which not only is mostly driven by $^{H}T_{1\rho}$ but also includes relaxation contributions from carbon nuclei (33). The magnetization of the carbons in PPG units (the assigned peaks with the highest intensity) was recorded as a function of the contact time included in the CP/MAS sequence (the plots are shown in Fig. 3a). It is noteworthy that those measurements included t_c as long as 100 ms; this was only made possible because the available electronics supports high power experiments. T_{CH} and $^{H}T_{1\rho}$ of the carbon nuclei, which have been obtained by fitting Eq. 2 to the experimental data, are presented in Table I. The curves shown in Fig. 3a represent the functions obtained from the corresponding least-squares fits (see Materials and Methods for details). The first part of the curve is associated to fast processes in protonated carbons, and the maximum magnetization is reached within a short time (short T_{CH}). The decrease of the curve is mainly dependent on $^{H}T_{1\rho}$ only when local magnetic field fluctuations in the kHz frequency range are induced by molecular motion, not by H–H spin-diffusion. Secondly, $^{H}T_{1\rho}$ data were measured by recording ^{13}C signals as a function of the ^{1}H spin-lock time (t) before the CP period. H–H spin-diffusion was minimized because CP duration was limited to only 400 μs. Figure 2b shows the

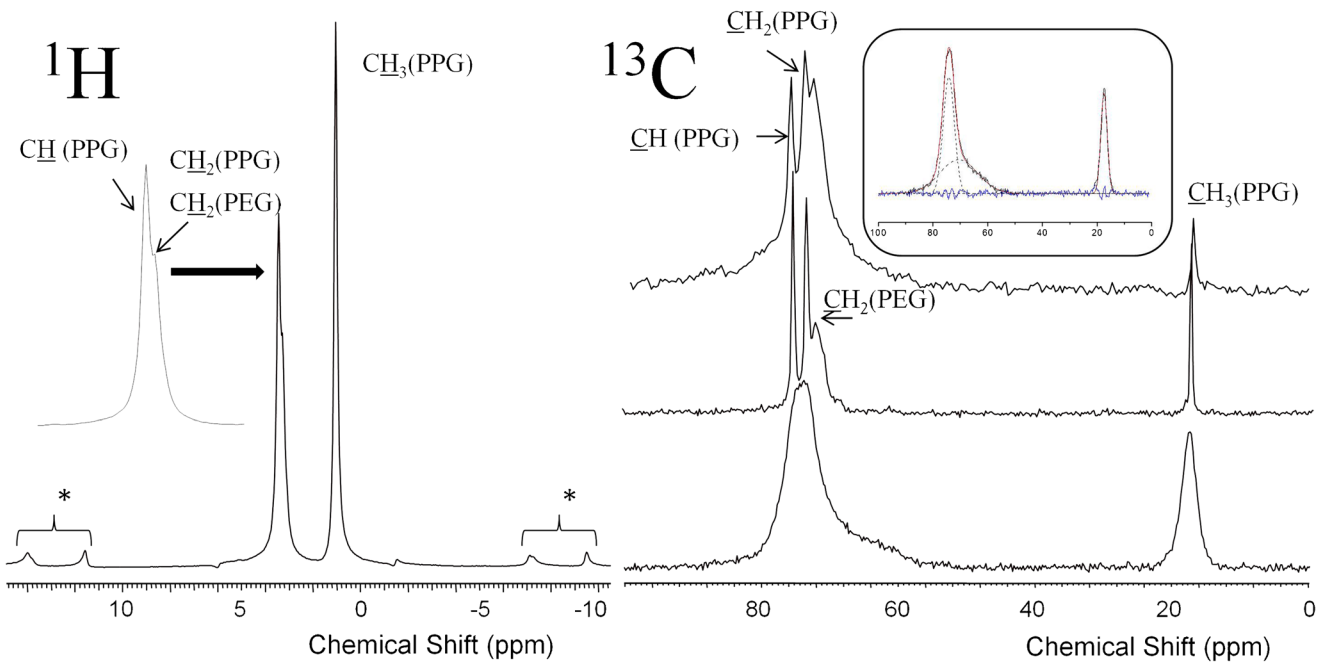

Fig. 2. ^{1}H MAS spectrum of PLX (left). Asterisk denotes spinning side bands. ^{13}C CP spectrum recorded in the static mode (bottom) and CP/MAS spectra obtained from PLX with the following contact times: 1 ms (middle) and 300 μs (top) (right). The inset shows the experimental (black color) and computed (red color) static spectra; the Gaussian curves (dotted lines) used in the deconvolution and the linear regression fit residues (blue lines)

plots of the magnetizations recorded from the different carbon nuclei as a function of t. Table I presents the results obtained by fitting Eq. 3 to the experimental data. At first, Fig. 3a, b enables noticing that PPG and PEG units follow different mobility regimes in the kHz frequency, which is the frequency range probed by $^{H}T_{1\rho}$. However, Fig. 3b shows that magnetization recorded from methine and methylene carbons in PPG units display an anomalous behavior. The decays are clearly nonexponential, which indicates multiple relaxation behavior; nevertheless, unexpected magnetization oscillations occurred when t was set from 2 to 5 ms. This behavior is related with heteronuclear dipolar coupling involving C and H spin pairs and the transient oscillations depend on the corresponding dipolar coupling strength (34); further elucidation is beyond the scope of the present work. The fitted exponential decays and the corresponding estimates of the time constants for the magnetization decrease recorded for t in the intervals 0–1 and 5–14 ms are shown in Fig. 3b and Table I, respectively.

Large differences in $^{H}T_{1\rho}$ were obtained between PPG and PEG domains (more than one order of magnitude). These results, as well as TCH, correlate well with PPG and PEG being the amorphous and crystalline components of PLX, respectively, as previously hypothesized.

Because the relaxation times have been measured about 80°C above the T_g of PLX, it is reasonable to consider that long $^{H}T_{1\rho}$ values (Table I) are due to motions on the high-frequency side of the $^{H}T_{1\rho}$ minimum, that is under fast motion conditions $\varpi_1^2\tau_c^2 << 1$ where τ_c is the rotational correlation time (the time that a chemical species takes to rotate one radian and, therefore, a direct measure of the rate of motion) and ω_1 ($62.5 \times 2\pi \times 10^3$ rad/s) is the spin-lock field (35). On the other hand, PEG data are consistent with motions on the low-frequency side of the $^{H}T_{1\rho}$ minimum that are expected to be dominant in crystalline regions.

$^{H}T_{1\rho}$ data have been previously obtained both for amorphous PZQ and PVP (Table I) (17).

^{13}C Spectral Elucidation of PVP. The ^{13}C CP/MAS TOSS solid-state NMR spectrum of PVP was previously shown; its broad signals, typical of an amorphous polymer, were assigned (17).

^{13}C Spectral Elucidation of PZQ. The full assignment of ^{13}C spectrum of PZQ has been previously performed (8,17). Figure S2 (*Supplementary Material*) shows ^{13}C CP/MAS spectra run with or without the TOSS sequence (27). The resonances are labeled according to the PZQ carbon numbering presented in Scheme 1. The signals are all narrow, as expected from a microcrystalline powdered drug.

Amorphous PZQ has been studied and compared with the crystalline form (8). It was revealed that, upon amorphization, the most affected resonances are those from carbonyl C2, carbons C1 and C14 (next to the carbonyl group) and C4 and C5 (next to the nitrogen atoms). The parameters of the Gaussian functions used to deconvolute C2 signals recorded from pure PZQ are given in Table II. The three signals that describe C2 resonances from crystalline PZQ combine into one broad signal in the spectrum of amorphous PZQ (FWHM 257 Hz). Accordingly, it has been suggested that the dominant conformer in amorphous PZQ should be different from those in the crystalline state (8).

DSC Studies of Binary and Ternary Solid Dispersions and Physical Mixtures

DSC Studies of PLX/PZQ Solid Dispersions and Physical Mixtures

Figure S3 (*Supplementary Material*) shows the thermograms obtained for PZQ/PLX (1:1) as SD (Fig. S3A) or physical mixture (Fig. S3B). The DSC curves present sharp endothermic peaks ($T = 50.97$ and 50.06°C, respectively) corresponding to the PLX melting point, revealing its crystalline state. A decrease of the PZQ fusion onset temperature in the SD was detected which may be consistent with a molecular interaction with PLX or due to the fact that PZQ ($T_m = 142.52$°C) has dissolved in PLX ($T_m = 49$°C) at high temperature during thermal analyses.

DSC Studies of PVP/PLX/PZQ Solid Dispersions and Physical Mixtures

The thermograms obtained from SDs and PMs are shown in Fig. 4. These data present endothermic signals characteristic of a semi-crystalline copolymer: thermal signatures attributed to PLX melting (49°C) and to the T_g of PLX (−61°C), respectively. Besides, signals are detected at about 130°C, indicating that PZQ has remained, at least partly, in the crystalline state. The thermal behavior of PVP K30 is that expected for amorphous, hygroscopic polymers with broad endothermic curves ranging from 20 to 100°C (high intensity at ~58°C) which were previously assigned to a dehydration event of PVP (31,36).

Therefore, both SDs and PMs consist of major crystalline PLX domains and amorphous PVP regions. This DSC result provides evidence that PLX is almost immiscible with both PVP and PZQ, most possibly just acting as plasticizer. Such low miscibility involving the two polymers is expected accounting for the few PLX hydroxyl end groups able to form hydrogen bonds with the PVP carbonyl groups.

The thermograms of PVP/PLX/PZQ SDs and PMs show more than one endothermic signal in the region 45 to 100°C (comprising the melting temperature of PLX) that we tentatively assigned to possible interaction of PLX with PVP. In addition, it is expected that a small fraction of PLX remains dissolved into PVP and, consequently, its T_g shifts marginally to lower temperature values compared to neat PLX. On one hand, the use of low heating rate allows identifying multiple peaks in the DSC thermogram, and on the other, it reduces significantly the relative amplitude of the signal associated to T_g (of PVP). In this scenario, three possible explanations could be projected: (a) melting–recrystallization–remelting mechanisms (37) or (b) the occurrence of at least two distinct crystal populations (38), or (c) a coexistence of amorphous and crystalline PZQ. All hypotheses remain frequently open questions in the literature, and it is outside the scope of this study to assess the most plausible

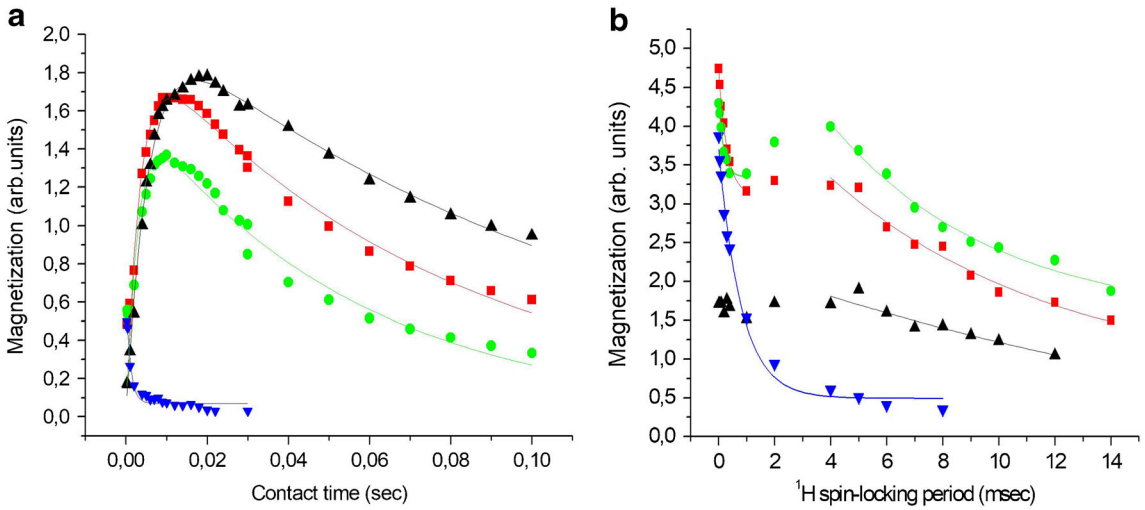

Fig. 3. Plots of the magnetization recorded from the carbons in PPG units (CH_2 (filled square), CH (filled circle), and CH_3 (filled triangle)) and in PEG units (CH_2 (filled inverted triangle)) (the highest intensity of the assigned peaks), as a function of **a** contact time during the cross polarization RF sequence and **b** duration of ^{1}H spin-locking before the cross polarization period. The curves represent functions from least-squares fits to obtain the following relaxation parameters of the indicated carbon nuclei. **a** T_{CH} and $^{H}T_{1\rho}$. **b** $^{H}T_{1\rho}$ (see the "*Supplementary Material*" section for details)

one for the ternary system under evaluation. However, it must be pointed out here that NMR data shown in the next section demonstrate the presence of both PZQ forms. Moreover, it could be anticipated that the detection of a signal attributed to T_g of PVP can indicate that a small amount of PLX remains dissolved into PVP does explaining also the detection of two PLX melting signals (about 49 and 52°C) and it could be a manifestation of heterogeneity of SD or eventually a phase separation.

In the DSC thermograms, the characteristic endothermic peaks assigned to PZQ melting were broadened and shifted toward lower temperatures, presenting also decreased intensity, in both PMs as well as in SDs. This could be ascribed to higher polymer concentration and consequent increased miscibility of molten PZQ in polymeric medium. However, it could be recognized that the result of DSC study alone could not confirm the formation of PZQ amorphous state in the SDs.

Solid-State NMR of Binary and Ternary Solid Dispersions and Physical Mixtures

^{1}H and ^{13}C Solid-State NMR of PLX/PZQ Solid Dispersions and Physical Mixtures

The ^{1}H spectra obtained from binary SD and PM (both 1:1, *w*/*w*) are shown in Fig. S4A (see *Supplementary Material*). These spectra are similar to the one presented for pure PLX (Fig. 2).

Figure 5a shows the ^{13}C spectrum of SD. A small and narrow signal is assigned to PEG methylene groups (δ 71.07 ppm). The intensity of C14 and C5 overlapping resonances is lower when compared with the spectrum obtained for pure PZQ (Fig. S2, see *Supplementary Material*).

Table II presents FWHM and weight (%) of the three Gaussian functions used to deconvolute C2 signals from crystalline PZQ and PZQ at PLX/PZQ (1:1) SD. Different

Table I. Time Constants for the ^{13}C Magnetization Build-up Under CP (T_{CH}, ms) and Spin-Lattice Relaxation Time in the Rotating Frame ($^{H}T_{1\rho}$, ms) Obtained for PLX. Equations 1 or 2 Were Used to Fit the Experimental Data. The Errors Related with the Fittings Are Presented. Some PVP and PZQ Data Are Also Shown (17)

	PLX				PVP (17)	PZQ (17)
	PPG			PEG		
	CH	CH_2	CH_3	CH_2	C4	C3
T_{CH} (Eq.1)	2.79 ± 0.41	3.32 ± 0.30	5.32 ± 0.16	–[a]	–	–
$^{H}T_{1\rho}$ (Eq.1)	55.06 ± 5.91	76.50 ± 5.82	114.87 ± 4.19	1.09 ± 0.16	15.42 ± 0.90	9.73 ± 0.98[b]
$^{H}T_{1\rho}$ (Eq.2)	0.18 ± 0.03[c]	0.30 ± 0.03	~ 23	0.81 ± 0.08	–	–
	4.9 ± 1.2[d]	[c]5.3 ± 1.6[d]				

[a] Too short to be obtained
[b] In the amorphous state
[c] From data in the interval 0–1 ms
[d] From data in the interval 5–14 ms

Table II. Parameters of the Gaussian Functions Used to Deconvolute C2 Signals Recorded from Pure PZQ (Either Crystalline or Amorphous) and from PLX/PZQ (1:1) SD. Data Obtained from Deconvolutions of the ^{13}C CP/MAS Sub-spectra from PVP/PLX/PZQ SDs Are Also Shown, Namely, Prameters of the Gaussian Functions Used to Fit the Indicated Carbon Signals *via* the Least-Squares Method

	δ (ppm)	FWHM (Hz)	Peak area (%)
PZQ			
Crystalline (8), C2	165.24 ± 0.01	71 ± 2	~ 8
	164.20 ± 0.03	162 ± 5	~ 25
	161.73 ± 0.01	124 ± 1	~ 67
Amorphous (17), C2	164.36 ± 0.01	257 ± 2	100
PLX/PZQ (1:1), C2			
	165.61 ± 0.05	35 ± 9	~ 2
	164.66 ± 0.05	141 ± 6	~ 32
	162.13 ± 0.01	97 ± 2	~ 66
PVP/PLX/PZQ (1:1:1)			
C2	165.52 ± 0.07	76 ± 8	~ 9
	164.23 ± 0.05	110 ± 6	~ 19
	162.72 ± 0.02	134 ± 2	~ 72
C9,10,11	126.88 ± 0.06	249 ± 7	1.87 ± 0.04[a]
C7,8,12	134.49 ± 0.12	239 ± 14	0.93 ± 0.05[a]
PVP/PLX/PZQ (2:1:1)			
C2	165.68 ± 0.03	72 ± 5	~ 15
	164.02 ± 0.03	115 ± 5	~ 32
	162.49 ± 0.02	115 ± 3	~ 53
C9,10,11	127.48 ± 0.05	223 ± 5	1.74 ± 0.04[a]
C7,8,12	134.41 ± 0.07	231 ± 9	1.17 ± 0.04[a]

[a] Arbitrary units

PZQ species may contribute to the amorphous PZQ spectrum: PZQ isomers (*R* and *S* enantiomers, with the quiral center at C3) and the corresponding *cis* and *trans* conformers. The chemical shift of C2 (about 164 ppm) is the average value that reflects the distribution of electronic environments due to lacking of short-range order. Therefore, compared to the crystalline PZQ parameters, changes in C2 NMR data may indicate coexistence of both PZQ forms.

Table II reveals marginal differences in the areas of the resonances at about 165 and 164 ppm along with lower FWHM for the three signals of PZQ as PLX/PZQ formulation. Hence, these data are consistent with amorphous PZQ in the binary SD being absent or below the ssNMR detection limit. Figure S5 (*Supplementary Material*) shows spectra from both SD and PM, for comparison; other than broadening of the PEG peak in PM spectrum, no major differences are noticed between the signals recorded from PM and SD samples. This result correlates well with the PZQ dissolution efficiency of about 73% after 180 min obtained from both SD and PM samples. It is reasonable to expect a crystal size decrease of the drug as binary PMs. Such effect explains the corresponding PZQ dissolution increase compared to raw PZQ (Fig. 1).

^{1}H and ^{13}C Solid-State NMR of PVP/PLX/PZQ Solid Dispersions and Physical Mixtures

The ^{1}H NMR spectra of ternary (PVP/PLX/PZQ) SDs and PMs at 1:1:1 and 2:1:1 are displayed in Fig. S4B (see *Supplementary Material*). Similarly to pure PLX, the resonances (δ 1.07, 3.31, 3.47 ppm) are assigned to CH_3, CH_2, and CH from PPG units, respectively; the signal at 3.31 ppm includes the contribution from PEG methylene groups. Other weaker peaks are from spinning side bands, as already noticed on ^{1}H PLX spectrum. The signals assigned to OH groups in SDs are observed at 4.57 and 4.36 ppm, respectively. These signals are mostly from sorbed water by the hydrophilic polymer (PVP), but the spectrum of the SD with higher PVP content shows a signal broadening and a shift to lower frequency of resonance. Water may be present as free, bound, or entrapped water molecules. Free water molecules give resonances at about 4.5–4.8 ppm but, when hydrogen bonds are broken as in bound or entrapped molecules, lower chemical shifts are detected. This is the case of the OH signal at δ 4.36 ppm. Hence, this observation is consistent with the presence of a smaller number of hydrogen bonds. In addition, the signal broadening points to a large distribution of electronic environments. OH signals recorded from PMs are assigned to free water molecules (δ 4.53 ppm) and are more intense in the 2:1:1 spectrum. Noteworthy, no OH signal has been detected either from raw PLX or from binary formulations.

Figure 5b shows the ^{13}C spectra obtained from PVP/PLX/PZQ SDs at 1:1:1 and 2:1:1. Similarly to the binary SD, the signal from PEG methylene groups is small and narrow (δ 71.07 ppm). As for PZQ, C2 signals present a line shape dependence on the contribution of three components, previously identified in the spectrum of the pure drug (Table II). The inset in Fig. 5b enables comparing the PZQ sub-spectra obtained from SDs with different weight ratio (1:1:1 and 2:1:1). The signals recorded from C2 and the aromatic group were deconvoluted using Gaussian functions *via* the least-squares method; input chemical shifts and FWHM for C2 components were those derived from crystalline PZQ (Table II). The Gaussian curves are shown in Fig. 5b, and all the corresponding parameters are listed in Table SI (chemical shift, FWHM and area, *Supplementary Material*). Narrow and broad signals are present in agreement with crystalline and amorphous PZQ contributions, respectively. The parameters of the Gaussian functions assigned to the aromatic group of amorphous PZQ (broader curves) and those used to deconvolute the carbonyl C2 signals are both presented in Table II. The areas of C2 signals show a strong dependence on the formulation under analysis, which is not noticed as far as the chemical shifts are concerned. At first, it seems correct to evaluate the contribution of the amorphous drug based on the area of the signal at about 164 ppm, because this is the chemical shift of C2 recorded from raw PZQ in amorphous form (Table II). Indeed, the CP technique can provide quantitative information between different species when the ^{13}C relative intensities of the signals under comparison originate from carbons of the same multiplicity. The contribution of the broad curve at about 164 ppm increases from 19 to 32% by increasing the PVP amount (Table II). Therefore, based on the areas obtained for C2 signals, the preliminary conclusion is that amorphous PZQ increases with PVP. However, for each SD, Table SI (*Supplementary Material*) shows that the areas of the two broader signals represent around 28% of the total area of the aromatic group signals (C7 to C12). This result is consistent

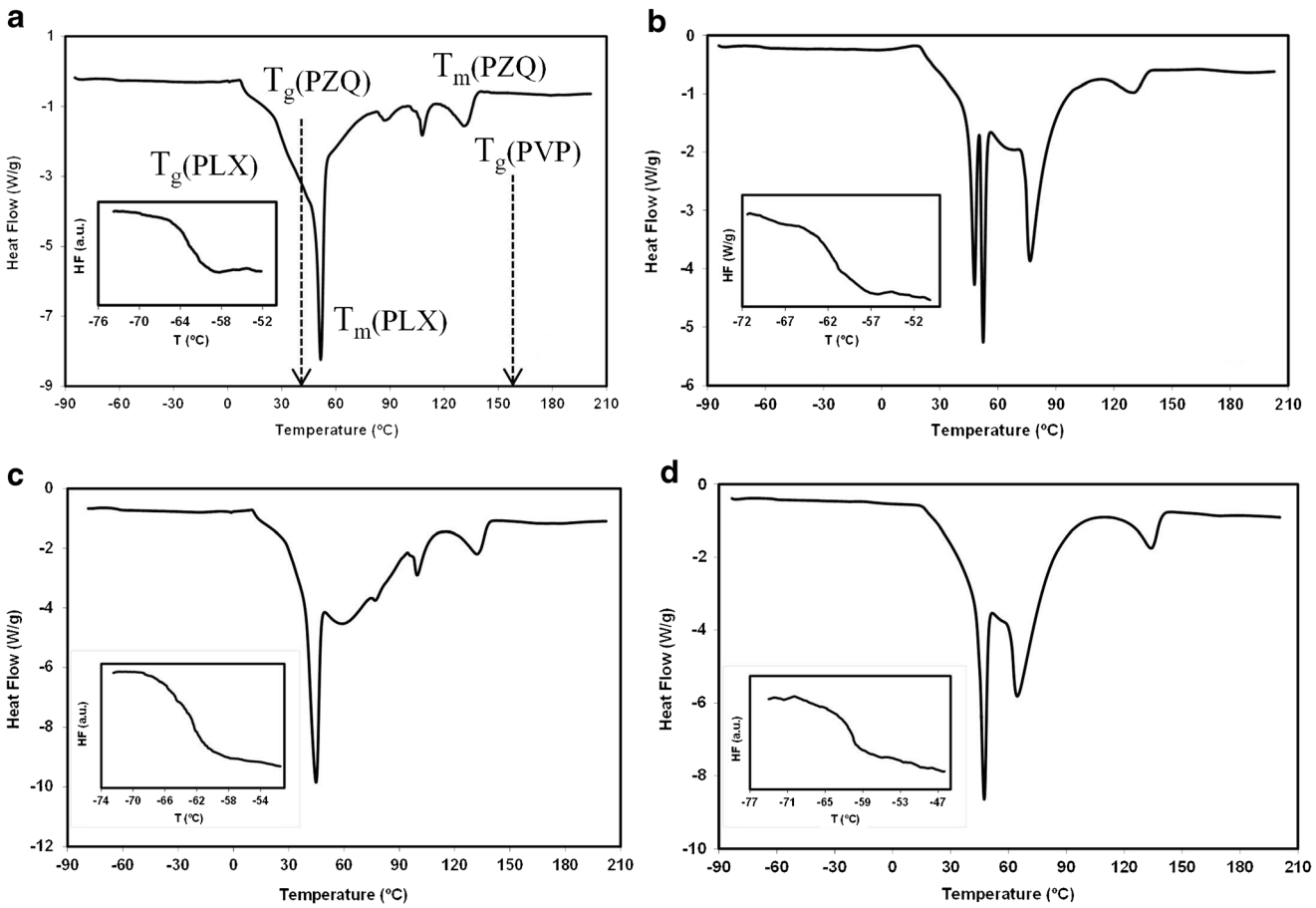

Fig. 4. Thermograms of PVP/PLX/PZQ SDs at 1:1:1 (**a**) and 2:1:1 (**b**) (top). Thermograms of PVP/PLX/PZQ PMs at 1:1:1 (**c**) and 2:1:1 (**d**) (bottom). The insets show the PLX glass transitions regions corresponding to the following T_g values: − 63.2°C (**a**), − 61.6°C (**b**), − 62.4°C (**c**), and − 61.2°C (**d**). PZQ and PLX T_m peaks are indicated. Arrows show PZQ and PVP T_g regions. Signal convention is exo up

with an amount of amorphous PZQ being comparable in both SDs.

DE at 180 min has increased from 80.5 ± 0.5 to 82.5 ± 0.1% by changing the PVP/PLX/PZQ SD formulation from 1:1:1 to 2:1:1. Therefore, DE does not correlate with concentration of amorphous PZQ. In addition, the strong dependence of the carbonyl C2 signals (FWHM and area) on the formulation composition must have an explanation beyond the presence of amorphous drug. Higher PZQ dissolution as ternary SD 2:1:1 (Fig. 1) has to be due to another feature. A possible explanation would be the presence of distinct crystal populations, one of the hypotheses consistent with the observation of several different melting peaks detected in DSC thermograms (Fig. 4b).

Under favorable conditions, NMR relaxation can be exploited to assist the interpretation of systems exhibiting regions with different morphologies. Two NMR relaxation filters have been used for that purpose which are based on spin-spin relaxation ($^{H}T_2$) and $^{H}T_{1\rho}$ (39). In general, hydrogen mobility in the kHz frequency range, probed by those relaxation times, is much higher in amorphous than in crystalline drugs.

The coexistence of PZQ domains with different mobility is demonstrated by comparing the spectrum run under the usual CP sequence with the one obtained with a sequence that includes a delay of 15 μs after the 90° RF pulse in the ^{1}H channel (Fig. 6 B). This sequence enables eliminating, at least partly, more rigid crystalline PZQ contribution characterized by shorter proton $^{H}T_2$. Signals of amorphous species are expected to be enhanced. An intensity decrease of several aromatic and carbonyl resonances is observed from the SD at 1:1:1. Clearly, for the SD at 2:1:1, it is observed (a) a strong line narrowing, more pronounced in the aromatic low-magnetic field region, and (b) the relative intensity decrease of PVP C2,3 resonances (at 43 ppm) that are superimposing C1 and C4 signals from crystalline PZQ (at about 47 and 45 ppm), respectively (8). Therefore, both (a) and (b) observations are explained by the partly suppression of signals from the most rigid crystalline domains, with the shortest $^{H}T_2$.

Return to thermal equilibrium of the magnetization in the rotating frame is controlled by the time constant $^{H}T_{1\rho}$, which is about 6 and 140 ms for C3-*H* (or C10-*H*) in amorphous and crystalline PZQ, respectively (8). Therefore, delaying the contact time by 4 ms in the CP experiment is expected to favor the observation of crystalline PZQ. Figure 6 shows the ^{13}C CP/MAS spectra of the PVP/PLX/PZQ SDs at 1:1:1 and 2:1:1 recorded without (Fig. 6 A) or with a $^{H}T_{1\rho}$ filter of 4 ms in the ^{1}H channel, before the RF contact pulse (Fig. 6 C). Under this condition, the signal intensity of

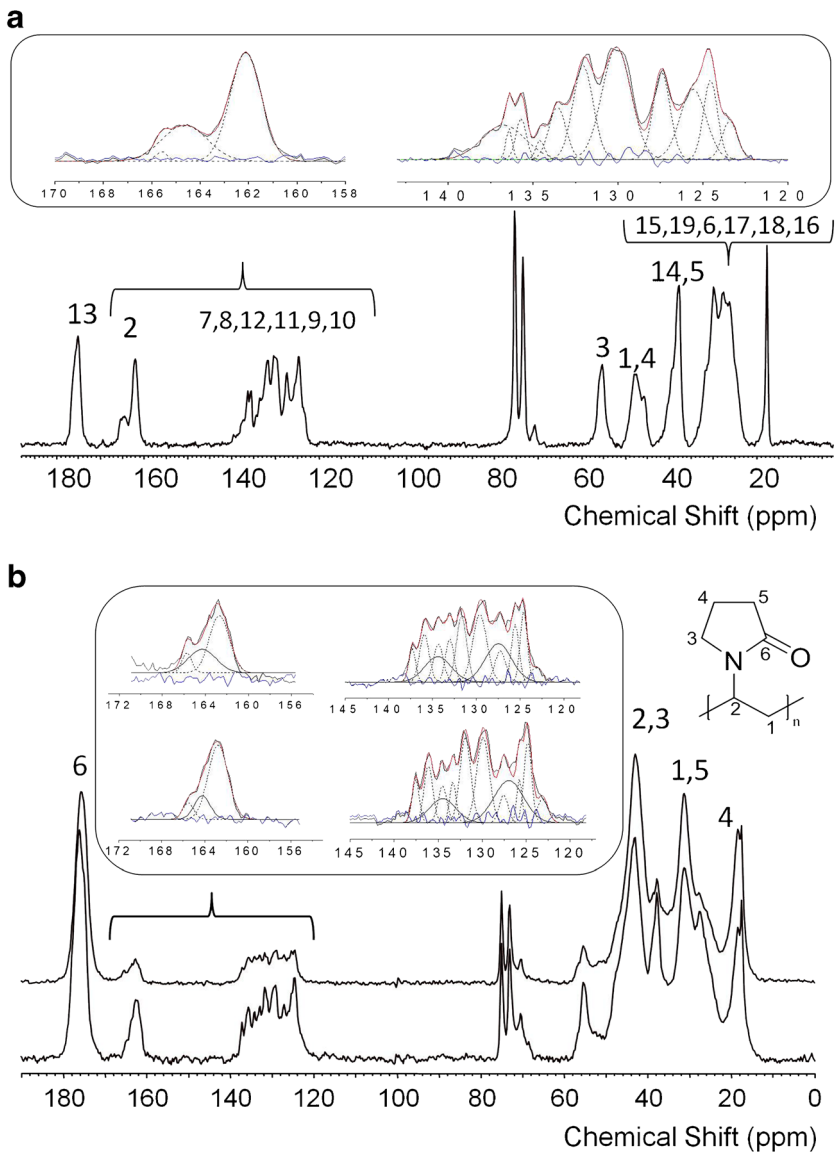

Fig. 5. **a** ^{13}C CP/MAS spectrum of PZQ/PLX (1:1) SD. The inset shows the experimental (black color) and computed (red color) sub-spectra; the Gaussian curves (dashed black lines) used in the deconvolution and the linear regression fit residues (blue lines). The assignment of PZQ resonances is indicated. **b** ^{13}C CP/MAS spectra of PVP/PLX/PZQ SDs with the following weight ratios: 1:1:1 (bottom) and 2:1:1 (top). The inset displays ^{13}C CP/MAS experimental and computed sub-spectra, shown in black and red colors, respectively, the linear regression fit residues (blue) and the curves representing the Gaussian functions used to deconvolute the experimental sub-spectra (dashed and solid black lines). The assignment of PVP resonances is indicated

amorphous PZQ has significantly reduced, whereas the crystalline component has retained most of its intensity. The effect is particularly noticed in the high magnetic field region of aromatic carbon resonances from SD at 2:1:1. As for highly mobile PLX, the strong decrease of the signals is related to the fact that the time constant for the ^{13}C magnetization build-up (T_{CH}; Table II) is close to 4 ms, which is the selected duration for ^{1}H magnetization in the rotating frame decrease, before the CP period. Concerning PVP in SD at 2:1:1, not all the carbon nuclei reveal similar behavior; C1,5 and C4 signals do show reduced intensity whereas C6 and C2,3 resonances remain intense. The broad OH resonance at about 4.3 ppm in the ^{1}H spectrum (FWHM 488 Hz; Fig. S4B, *Supplementary Material*) is consistent with the presence of bound water, most probably involving C6-*O* and/or C2,3-*N*. Consequently, these carbons, in a more rigid environment, are less affected than C1,5 and C4 by the inclusion of the $^{H}T_{1\rho}$ filter in the RF pulse sequence. Such effect is not observed for the SD at 1:1:1. In this case, all the PVP carbon signals display reduced intensity. In addition, the line width (146 Hz) and chemical shift (4.6 ppm) of the OH resonance indicate free water predominance (Fig. S4B, *Supplementary Material*).

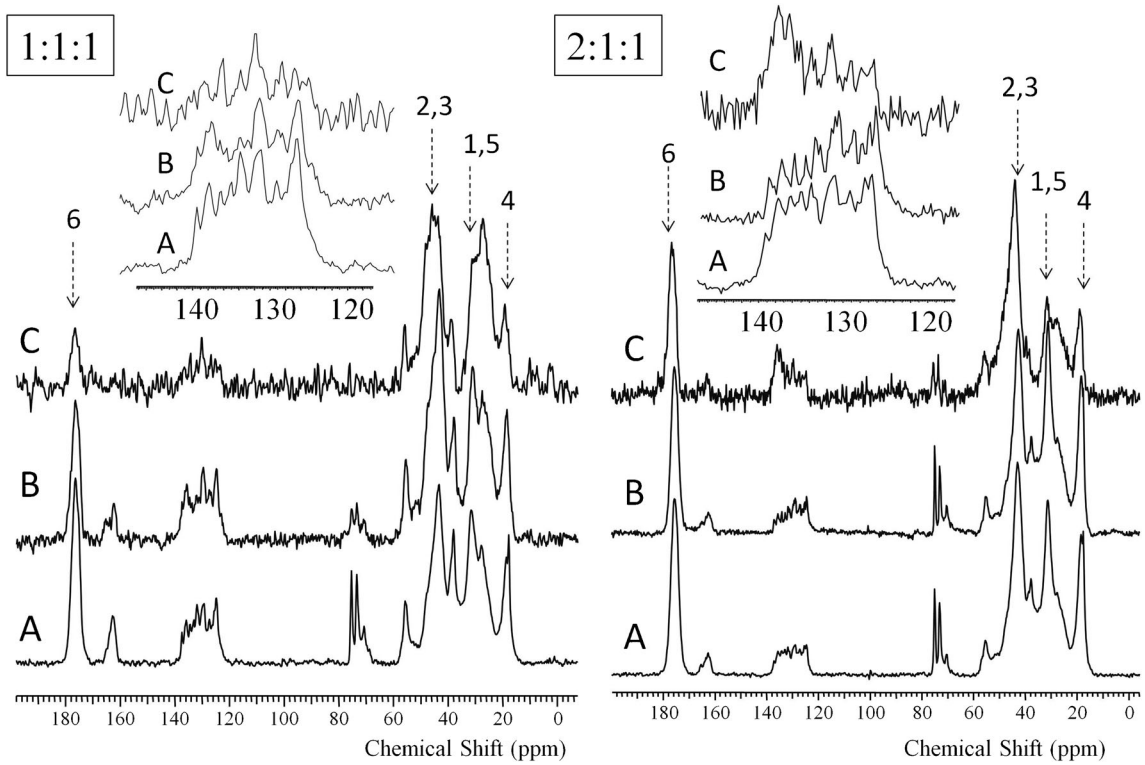

Fig. 6. ^{13}C CP/MAS spectra of PVP/PLX/PZQ SDs at 1:1:1 and 2:1:1 obtained as following: (A) with the standard CP RF sequence, (B) using a CP RF sequence that includes a delay of 15 μs after the 90° RF pulse in the ^{1}H channel, and (C) keeping ^{1}H magnetization spin-locked but delaying the contact period by 4 ms. Arrows indicate PVP spectral regions. The insets show magnifications of the aromatic carbon signals

In summary, we have obtained evidences for the coexistence of amorphous and crystalline PZQ in PVP/PLX/PZQ SDs. In addition, crystalline forms with different mobilities were detected.

Recently, solution and solid phases in a nanosuspension of piroxicam (PXC) and PLX 407 have been studied by ^{13}C solution-state and suspended-state NMR and Raman spectroscopies (32); evidence was presented for the solubility increase of a drug coexisting in nanoparticles in both amorphous and crystalline forms.

Figure S6 (*Supplementary Material*) shows the ^{13}C CP/MAS spectra obtained from PMs at 1:1:1 and 2:1:1. The spectra just display overlapping signals from the three isolated components, and no difference is noticed in the chemical shifts. The dissolution improvement of PZQ as ternary PMs (Fig. 1) may be related to the crystal size decrease of the drug.

No significant changes have been revealed in the NMR spectra recorded over 6 months from SDs (kept at about 5°C). Therefore, under the NMR detection limit, those samples are stable at least during that period. This evidence will be helpful for the stability evaluation of this solid-state pharmaceutical preparation.

CONCLUSIONS

Propylene glycol and ethylene glycol constitute the amorphous and crystalline PLX components, respectively, as shown for the first time using ssNMR.

PZQ dissolution efficiency has been improved both as PMs and SDs. The enhancement was higher for SDs. A crystal size decrease of PZQ, by maximizing the PZQ surface area in contact with the solvent, may account for the PZQ behavior as binary and ternary PMs.

DSC profiles of *binary samples* (endothermic signal at 132°C) and ^{13}C CP/MAS NMR spectra revealed the presence of crystalline PZQ. Endotherms at about 50°C show that PLX remained partially crystalline in all the samples. Narrow PPG ^{1}H and ^{13}C NMR signals are consistent with the assignment of PPG units to the soft, amorphous, semi-crystalline copolymer regions.

NMR data from *ternary SDs* show both broad and narrow superimposed signals in agreement with the coexistence of amorphous and crystalline PZQ, respectively. Such result could not be confirmed by DSC. Therefore, using PLX did not improve the stability of amorphous PZQ that was only detected in the presence of PVP. PZQ interaction with PVP leads to the stabilization of the amorphous drug while the presence of PLX favors the drug crystallization and most probably the formation of particles with PPG in the inner core close to PZQ. PZQ miscibility with PVP may be due to the interaction of PZQ polar groups with the functional groups of PVP (*e.g.*, carbonyls) and make van der Waals or hydrogen bonds. Such bonds would inhibit in part PZQ recrystallization. In addition, PVP and PLX could contribute to get better drug wettability as a consequence of the surface tension lowering effect of both polymers. However, DSC supported that these polymers did not form homogeneous mixtures. DSC and ssNMR gave evidences for the presence of distinct crystal populations in ternary SDs.

In summary, SDs, prepared using the solvent evaporation technique in the presence of PVP, provided a route to improve PZQ dissolution. Dissolution efficiency has shown a dependence on the carrier concentration. PZQ dissolution has increased from binary to ternary SDs, that is, with PVP concentration. The dissolution PZQ enhancement is assigned here to the presence of amorphous PZQ, which was only detected in the presence of PVP. This is consistent with the role of PVP as an amorphous PZQ enhancer.

The fact that no significant changes have been noticed in the NMR spectra of SDs is an encouraging observation in the context of the drug storage issue, but other testing under long-term stability are needed.

ACKNOWLEDGEMENTS

J.P thanks CONICET (Argentina) for a Ph.D. fellowship. The authors thank Msc. E. Costa for the acquisition of some DSC and NMR data during his fellowship period (FCT, BL-CQE/2015-011) and Dr. M.J. Ferreira for NMR assistance.

Funding Information

Thanks are due for financial support to Fundação para Ciência e Tecnologia (FCT, Portugal, projects RECI/QEQ-QIN/0189/2012 and UID/QUI/00100/2013) and UNR (Argentina), CONICET (Argentina), and MINCYT (Argentina) (PICT 1078).

REFERENCES

1. WHO, 2017a. World Health Organization. Media Center. Schistosomiasis. http://www.who.int/mediacentre/factsheets/fs115/en/. **Accessed 10 Aug 2017**.
2. WHO, 2017b. World Health Organization. Schistosomiasis. Strategy. http://www.who.int/schistosomiasis/strategy/en/. **Accessed 10 Aug 2017**.
3. Lindenberg M, Kopp S, Dressman JB. Classification of orally administered drugs on the World Health Organization model list of essential medicines according to the biopharmaceutics classification system. Eur J Pharm Biopharm. 2004;58(2):265–78. https://doi.org/10.1016/j.ejpb.2004.03.001.
4. De La Torre P, Torrado S, Torrado S. Preparation, dissolution and characterization of praziquantel solid dispersions. Chem Pharm Bull. 1999;47(11):1629–33. https://doi.org/10.1248/cpb.47.1629.
5. Frezza TF, Gremião MP, Zanotti-Magalhães EA, Magalhães LA, Ribeiro de Souza AL, Allegretti SM. Liposomal-praziquantel: efficacy against Schistosoma mansoni in a preclinical assay. Acta Trop. 2013;128(1):70–5. https://doi.org/10.1016/j.actatropica.2013.06.011.
6. Meyer T, Sekljic H, Fuchs S, Bothe H, Schollmeyer D, Miculka C. Taste, a new incentive to switch to (R)-praziquantel in schistosomiasis treatment. PLoS Negl Trop Dis. 2009;3(1):e357. https://doi.org/10.1371/journal.pntd.0000357.
7. Perissutti B, Passerini N, Trastullo R, Keiser J, Zanolla D, Zingone G, et al. An explorative analysis of process and formulation variables affecting comilling in a vibrational mill: the case of praziquantel. Int J Pharm. 2017;533(2):402–12. https://doi.org/10.1016/j.ijpharm.2017.05.053.
8. Arrúa EC, Ferreira MJG, Salomon CJ, Nunes TG. Elucidating the guest-host interactions and complex formation of praziquantel and cyclodextrin derivatives by ^{13}C and ^{15}N solid-state NMR spectroscopy. Int J Pharm. 2015;496(2):812–21. https://doi.org/10.1016/j.ijpharm.2015.11.026.
9. Chaud MV, Tamascia P, de Lima AC, Paganelli MO, Gremião MPD, de Freitas O. Solid dispersions with hydrogenated castor oil increase solubility, dissolution rate and intestinal absorption of praziquantel. Braz J Pharm Sci. 2010;46(3):473–81. https://doi.org/10.1590/S1984-82502010000300010.
10. Bagade O, Shete A, Dhole S, Pujari R, Raskar V, Kharat P. Design and statistical optimisation of praziquantel tablets by using solid dispersion approach. Asian J Pharm. 2015;9(2):83–92. https://doi.org/10.4103/0973-8398.154689.
11. Dametto PR, Dametto AC, Polese L, Ribeiro CA, Chorilli M, de Freitas O. Development and physicochemical characterization of solid dispersions containing praziquantel for the treatment of schistosomiasis. J Therm Anal Calorim. 2017;127(2):1693–706. https://doi.org/10.1007/s10973-016-5759-1.
12. Baghel S, Cathcart H, O'Reilly NJ. Polymeric amorphous solid dispersions: a review of amorphization, crystallization, stabilization, solid-state characterization, and aqueous solubilization of biopharmaceutical classification system class II drugs. J Pharm Sci. 2016;105(9):2527–44. https://doi.org/10.1016/j.xphs.2015.10.008.
13. Tian Y, Jones DS, Andrews GP. An investigation into the role of polymeric carriers on crystal growth within amorphous solid dispersion systems. Mol Pharm. 2015;12(4):1180–92. https://doi.org/10.1021/mp500702s.
14. Gupta P, Kakumanu VK, Bansal AK. Stability and solubility of celecoxib-PVP amorphous dispersions: a molecular perspective. Pharm Res. 2004;21(10):1762–9. https://doi.org/10.1023/B:PHAM.0000045226.42859.b8.
15. Shah J, Vasanti S, Anroop B, Vyas H. Enhancement of dissolution rate of valdecoxib by solid dispersions technique with PVP K 30 & PEG 4000: preparation and in vitro evaluation. J Incl Phenom Macrocycl Chem. 2009;63(1-2):69–75. https://doi.org/10.1007/s10847-008-9490-9.
16. Joe JH, Lee WM, Park YJ, Joe KH, DH O, Seo YG, et al. Effect of the solid-dispersion method on the solubility and crystalline property of tacrolimus. Int J Pharm. 2010;395(1-2):161–6. https://doi.org/10.1016/j.ijpharm.2010.05.023.
17. Costa ED, Priotti J, Orlandi S, Leonardi D, Lamas MC, Nunes TG, et al. Unexpected solvent impact in the crystallinity of praziquantel/poly(vinylpyrrolidone) formulations. A solubility, DSC and solid-state NMR study. Int J Pharm. 2016;511(2):983–93. https://doi.org/10.1016/j.ijpharm.2016.08.009.
18. Devi DR, Sandhya P, Hari BV. Poloxamer: a novel functional molecule for drug delivery and gene therapy. J Pharm Sci Res. 2013;5:159–65.
19. Pitto-Barry A, Barry NPE. Pluronic® block-copolymers in medicine: from chemical and biological versatility to rationalisation and clinical advances. Polym Chem. 2014;5(10):3291–7. https://doi.org/10.1039/C4PY00039K.
20. Beck-Broichsitter M, Bohr A, Ruge CA. Poloxamer-decorated polymer nanoparticles for lung surfactant compatibility. Mol Pharm. 2017;14(10):3464–72. https://doi.org/10.1021/acs.molpharmaceut.7b00477.
21. Essa EA, Balata GF. Preparation and characterization of domperidone solid dispersions. Pak J Pharm Sci. 2012;25(4):783–91.
22. Rao M,M,Y, Khole I, Munjapara G. Characterization of solid dispersions of simvastatin with PVP K30 and Poloxamer 188. Ind J Pharm Edu Res. 2011;45:145–52.
23. Fousteris E, Tarantili PA, Karavas E, Bikiaris D. Poly(vinyl pyrrolidone)–poloxamer-188 solid dispersions prepared by hot melt extrusion. J Therm Anal Calorim. 2013;113(3):1037–47. https://doi.org/10.1007/s10973-012-2885-2.
24. Chen Z, Liu Z, Qian F. Crystallization of bifonazole and acetaminophen within the matrix of semicrystalline, PEO-PPO-PEO triblock copolymers. Mol Pharm. 2015;12(2):590–9. https://doi.org/10.1021/mp500661v.
25. United States Pharmacopeia and National Formulary (USP 30 NF 25). Rockville, MD: United States Pharmacopeial Convention; 2007.
26. Moura Ramos JJ, Taveira-Marques R, Diogo HP. Estimation of the fragility index of indomethacin by DSC using the heating and cooling rate dependency of the glass transition. J Pharm Sci. 2004;93(6):1503–7. https://doi.org/10.1002/jps.20061.

27. Dixon WT, Schaefer J, Sefcik MD, Stejskal EO, McKay RA. Total suppression of sidebands in CPMAS C-13 NMR. J Magn Reson. 1982;49(2):341–5. https://doi.org/10.1016/0022-2364(82)90199-8.
28. Kolodziejski W, Klinowski J. Kinetics of cross-polarization in solid-state NMR: a guide for chemists. Chem Rev. 2002;102(3):613–28. https://doi.org/10.1021/cr000060n.
29. Oo MK, Mandal UK, Chatterjee B. Polymeric behavior evaluation of PVP K30-poloxamer binary carrier for solid dispersed nisoldipine by experimental design. Pharm Dev Technol. 2015;22(1):2–12. https://doi.org/10.3109/10837450.2015.1116568.
30. Kolašinac N, Kachrimanis K, Homšek I, Grujić B, Đurić Z, Ibrić S. Solubility enhancement of desloratadine by solid dispersion in poloxamers. Int J Pharm. 2012;436(1-2):161–70. https://doi.org/10.1016/j.ijpharm.2012.06.060.
31. Chan S-Y, Chung Y-Y, Cheah X-Z, Tan EY-L, Quah J. The characterization and dissolution performances of spray dried solid dispersion of ketoprofen in hydrophilic carriers. Asian J Pharm Sci. 2015;10(5):372–85. https://doi.org/10.1016/j.ajps.2015.04.003.
32. Hasegawa Y, Higashi K, Yamamoto K, Moribe K. Direct evaluation of molecular states of piroxicam/poloxamer nanosuspension by suspended-state NMR and Raman spectroscopies. Mol Pharm. 2015;12(5):1564–72. https://doi.org/10.1021/mp500872g.
33. Hediger S, Emsley L, Fischer M. Solid-state NMR characterization of hydration effects on polymer mobility in onion cell-wall material. Carbohydr Res. 1999;322(1-2):102–12. https://doi.org/10.1016/S0008-6215(99)00195-0.
34. Reinsberg SA, Ando S, Harris RK. Fluorine-19 NMR investigation of poly(trifluoroethylene). Polymer. 2000;41(10):3729–36. https://doi.org/10.1016/S0032-3861(99)00518-2.
35. Koenig JL. Spectroscopy of polymers. 2nd ed. New York: Elsevier Science Inc; 1999.
36. Trastullo R, Dolci LS, Passerini N, Albertini B. Development of flexible and dispersible oral formulations containing praziquantel for potential schistosomiasis treatment of pre-school age children. Int J Pharm. 2015;495(1):536–50. https://doi.org/10.1016/j.ijpharm.2015.09.019.
37. Blundell DJ. On the interpretation of multiple melting peaks in poly(ether ether ketone). Polymer. 1987;28(13):2248–51. https://doi.org/10.1016/0032-3861(87)90382-X.
38. Alizadeh A, Richardson L, Xu J, McCartney S, Marand H, Cheung Y, et al. Influence of structural and topological constraints on the crystallization and melting behavior of polymers. 1. Ethylene/1-octene copolymers. Macromolecules. 1999;32(19):6221–35. https://doi.org/10.1021/ma990669u.
39. Nasu M, Nemoto T, Mimura H, Sako K. Development of qualitative and quantitative analysis methods in pharmaceutical application with new selective signal excitation methods for 13C solid-state nuclear magnetic resonance using 1H T1rho relaxation time. J Pharm Sci. 2013;102(1):154–61. https://doi.org/10.1002/jps.23345.